ARTICLE

doi:10.1038/nature13908

The contribution of *de novo* coding mutations to autism spectrum disorder

Ivan Iossifov[1]*, Brian J. O'Roak[2,3]*, Stephan J. Sanders[4,5]*, Michael Ronemus[1]*, Niklas Krumm[2], Dan Levy[1], Holly A. Stessman[2], Kali T. Witherspoon[2], Laura Vives[2], Karynne E. Patterson[2], Joshua D. Smith[2], Bryan Paeper[2], Deborah A. Nickerson[2], Jeanselle Dea[4], Shan Dong[5,6], Luis E. Gonzalez[7], Jeffrey D. Mandell[4], Shrikant M. Mane[8], Michael T. Murtha[7], Catherine A. Sullivan[7], Michael F. Walker[4], Zainulabedin Waqar[7], Liping Wei[6,9], A. Jeremy Willsey[4,5], Boris Yamrom[1], Yoon-ha Lee[1], Ewa Grabowska[1,10], Ertugrul Dalkic[1,11], Zihua Wang[1], Steven Marks[1], Peter Andrews[1], Anthony Leotta[1], Jude Kendall[1], Inessa Hakker[1], Julie Rosenbaum[1], Beicong Ma[1], Linda Rodgers[1], Jennifer Troge[1], Giuseppe Narzisi[1,10], Seungtai Yoon[1], Michael C. Schatz[1], Kenny Ye[12], W. Richard McCombie[1], Jay Shendure[2], Evan E. Eichler[2,13], Matthew W. State[4,5,7,14] & Michael Wigler[1]

Whole exome sequencing has proven to be a powerful tool for understanding the genetic architecture of human disease. Here we apply it to more than 2,500 simplex families, each having a child with an autistic spectrum disorder. By comparing affected to unaffected siblings, we show that 13% of *de novo* missense mutations and 43% of *de novo* likely gene-disrupting (LGD) mutations contribute to 12% and 9% of diagnoses, respectively. Including copy number variants, coding *de novo* mutations contribute to about 30% of all simplex and 45% of female diagnoses. Almost all LGD mutations occur opposite wild-type alleles. LGD targets in affected females significantly overlap the targets in males of lower intelligence quotient (IQ), but neither overlaps significantly with targets in males of higher IQ. We estimate that LGD mutation in about 400 genes can contribute to the joint class of affected females and males of lower IQ, with an overlapping and similar number of genes vulnerable to contributory missense mutation. LGD targets in the joint class overlap with published targets for intellectual disability and schizophrenia, and are enriched for chromatin modifiers, FMRP-associated genes and embryonically expressed genes. Most of the significance for the latter comes from affected females.

Autism spectrum disorder (ASD) is characterized by impaired social interaction and communication, repetitive behaviour and restricted interests. It has a strong male bias, especially in high-functioning affected individuals. The contribution from transmission has long been suspected from increased sibling risk[1], but more recently the role of germline *de novo* (DN) mutation has been established, first from large-scale copy number variation in simplex families[2–5], and subsequently from exome sequencing. The smaller DN variants observed by DNA sequencing pinpoint candidate gene targets[6–8]. These developments have promoted a new model for causation, and re-evaluation of sibling risk[9,10].

Here we report whole exome sequencing of the Simons Simplex Collection (SSC)[11] and an extensive list of DN mutated targets, including 27 recurrent LGD (nonsense, frameshift and splice site) targets. The size and uniformity of this study allow an unprecedented evaluation of genetic vulnerability to ASD. We subdivide target sets by mutation type (missense and LGD) and affected child status (gender and non-verbal IQ, to which we refer throughout as 'IQ'), and explore the overlap between target sets and their enrichment for certain gene categories. We make estimates of the number of genes vulnerable to a given mutation type and the proportion of simplex autism resulting from DN mutation for each affected subpopulation.

SSC sequencing and validation

We report on 2,517 of ~2,800 SSC families including ~800 that were previously published[6–8]. We sequenced 2,508 affected children, 1,911 unaffected siblings and the parents of each family. Within the SSC, the overall gender bias in affected individuals, 7 males to 1 female, is nearly twice that typically reported. Exomes were analysed at Cold Spring Harbor Laboratory (CSHL), Yale School of Medicine, and University of Washington (Extended Data Figs 1 and 2 and Supplementary Table 1). Pipelines were blind with respect to affected status. For uniformity, all data were reanalysed with the CSHL pipeline, allowing comparison of analysis tools. All calls were validated or strongly supported, as listed (Supplementary Table 2) and described (Methods).

Rates and targets of DN mutation

For greatest precision we measured DN rates in quad families (one affected and one unaffected child) over genomic positions at which all family members had ≥40× sequence coverage (Methods and Supplementary Table 3). This 'joint 40× region' in the SSC was 32 gigabases (Gb) in total, or 48% of the targeted exome, from 1,867 quads. DN events were shared by siblings 1% of the time (Supplementary Table 2); and 1% of mutations had nearby nucleotide positions altered, presumably by single mutagenic events[12–14] (Supplementary Table 4). The overall rate of base substitution is 1.8×10^{-8} ($\pm 10^{-9}$) per base pair (Supplementary Table 5).

Rates of DN synonymous mutation in affected (0.34 per child) and unaffected (0.33 per child) siblings do not differ significantly (Fig. 1). By contrast, LGD mutations occur at significantly higher rates in affected versus unaffected siblings (Fig. 1 and Extended Data Fig. 3). The rate of LGD mutations is 0.12 in unaffected siblings and 0.21 in affected

[1]Cold Spring Harbor Laboratory, Cold Spring Harbor, New York 11724, USA. [2]Department of Genome Sciences, University of Washington School of Medicine, Seattle, Washington 98195, USA. [3]Molecular & Medical Genetics, Oregon Health & Science University, Portland, Oregon 97208, USA. [4]Department of Psychiatry, University of California, San Francisco, San Francisco, California 94158, USA. [5]Department of Genetics, Yale University School of Medicine, New Haven, Connecticut 06520, USA. [6]Center for Bioinformatics, State Key Laboratory of Protein and Plant Gene Research, School of Life Sciences, Peking University, Beijing 100871, China. [7]Child Study Center, Yale University School of Medicine, New Haven, Connecticut 06520, USA. [8]Yale Center for Genomic Analysis, Yale University School of Medicine, New Haven, Connecticut 06520, USA. [9]National Institute of Biological Sciences, Beijing 102206, China. [10]New York Genome Center, New York, New York 10013, USA. [11]Department of Medical Biology, Bulent Ecevit University School of Medicine, 67600 Zonguldak, Turkey. [12]Department of Epidemiology and Population Health, Albert Einstein College of Medicine, Bronx, New York 10461, USA. [13]Howard Hughes Medical Institute, Seattle, Washington 98195, USA. [14]Department of Psychiatry, Yale University School of Medicine, New Haven, Connecticut 06520, USA.
*These authors contributed equally to this work.

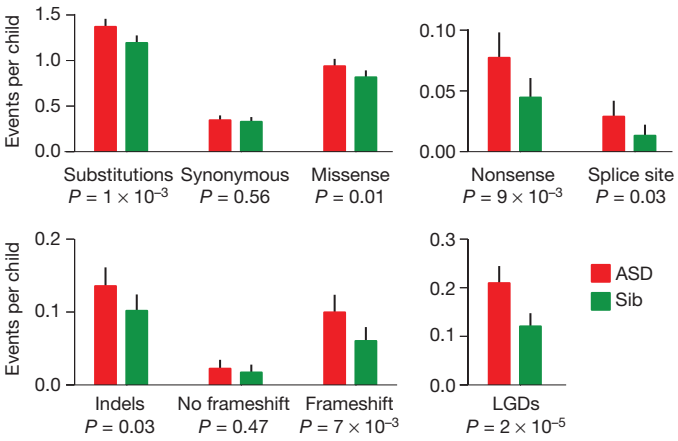

Figure 1 | Rates of *de novo* events by mutational type in the SSC. Rates per child are estimated from the 40× joint coverage target region, then extrapolated for the entire exome. Mutation types are displayed by class, and the combined rate for all LGDs is shown at the bottom right. For each event type, the significance between probands and unaffected siblings is given. Sib, unaffected siblings. The errors bar represent 95% confidence interval for the mean rates.

probands, an 'ascertainment differential' of $0.21 - 0.12 = 0.09$ ($P = 2 \times 10^{-5}$). Thus, we estimate ~43% (0.09 out of 0.21) of LGD events in probands contribute to ASD diagnoses. For DN missense, the rate is 0.82 for unaffected siblings and 0.94 for affected probands, an ascertainment differential of 0.12 ($P = 0.01$). We estimate only ~13% (0.12 out of 0.94) of DN missense events in probands contribute to ASD diagnoses. There is a wide confidence interval for the missense ascertainment differential (Supplementary Table 6); for this reason, we consider primarily the LGD events for our analysis and look on missense data as supporting.

To identify gene targets for DN mutation, we examined all family data including trios. We provide a complete list of all mutations (Supplementary Table 2) along with the number of mutations of each type in each gene (Supplementary Table 7). A total of 391 DN LGD mutations in 353 target genes were identified and validated in autism probands. Of these, 27 target genes were recurrent (Fig. 2). Among 1,500 missense targets in probands, 145 were recurrent.

We examined all alleles transmitted opposite a DN LGD target. We saw no instance in 391 observations in which the allele opposite an LGD target carried a rare transmitted LGD variant (in <1% of parental exomes), and only four in which such an allele carried a rare missense variant. Thus, the DN mutations do not generally cause homozygous loss-of-function of their target (Supplementary Table 8).

Confirming previous results[7,8,15], observed DN mutations arise three times as often in the paternal background, and mutation rates rise with age of either parent (Extended Data Fig. 4 and Methods). The latter may provide a partial explanation for increased autism rates in children born of older parents.

Functional clustering in target genes

Previous studies presented evidence of functional clustering in targets of DN LGD mutation in affected individuals[6–8,16]. Our larger data set was examined with an improved null 'length model' for mutation in which the probability of DN mutation in a gene is proportional to its length (Methods and Extended Data Fig. 5). We tested for enrichment within DN LGD and missense targets in probands and siblings for the following six classes: (1) FMRP target genes, with transcripts bound by the fragile X mental retardation protein[8,17]; (2) genes encoding chromatin modifiers; (3) genes expressed preferentially in embryos[18,19]; (4) genes encoding postsynaptic density proteins[20]; (5) essential genes[21]; and (6) genes identified as Mendelian disease genes[22] (Table 1, Supplementary Table 6 and Methods). These data provide the strongest evidence yet for overlap of DN LGD targets in affected probands with FMRP targets (55 observed versus 34.1 expected; $P = 4 \times 10^{-4}$) and chromatin modifiers (26 observed versus 11.8 expected; $P = 3 \times 10^{-4}$). We also observed signal from mutation in genes expressed in embryonic development[23] (65 observed versus 45.0 expected; $P = 2 \times 10^{-3}$). The latter signal comes mainly from the small number of female affected individuals (23 observed versus 8.5 expected from 67 LGD targets; $P = 5 \times 10^{-6}$). The 27 genes with recurrent LGDs show strong enrichment for FMRP targets (14 observed versus 2.6 expected; $P = 4 \times 10^{-8}$) and chromatin modifiers (6 observed versus 0.9 expected; $P = 2 \times 10^{-4}$). By contrast, no significant enrichment for these gene sets is seen for the DN LGD targets in unaffected siblings.

The 1,500 DN missense targets in probands are also enriched for FMRP targets and embryonically expressed genes. We observe 171 FMRP targets (144.8 expected; $P = 0.03$), and 220 embryonically expressed genes (191.4 expected; $P = 0.03$). As before, the signal for embryonically expressed genes comes almost entirely from the small number of female affected individuals (48 observed, 31.1 expected from 244 targets; $P = 0.002$). With the exception of chromatin modifiers, contributory DN missense and LGD mutations tend to strike similar functional classes of genes.

De novo mutation and IQ

Higher IQ probands are heavily skewed towards males[24]. For further analyses, we chose to divide the affected male population roughly in half into higher and lower IQ sets. We investigated whether higher IQ (>90) males comprise a population with a distinguishable genetic signature. There is a decreased ascertainment differential for DN LGD mutations in male children with higher IQ relative to other affected individuals (Extended Data Fig. 3 and Supplementary Table 6). This is not statistically significant over the joint 40× region. However, over the entire data set, the drop in IQ is 5 points for males with DN LGD mutation compared to those without mutation ($P = 0.01$; Fig. 2). The mean IQ of affected males with recurrent DN LGDs drops 20 points ($P = 0.00001$, Fig. 2). Significance is also evident as we examine targets by functional class. Males with LGD mutations in FMRP targets have an average 14-point drop ($P = 0.001$). This trend continues with LGD targets in the other functional classes—chromatin modifiers and embryonically expressed genes—but with reduced significance. We observe little signal from DN missense mutation, even in recurrent targets, either because these events are less likely to contribute or because they are less severe. Female probands show the same trends as males, but as they comprise a smaller population, the significance is weak (Fig. 2).

Further evidence for a distinguishable signature among the higher IQ comes from the functional enrichment within DN target gene sets. LGD targets in females are enriched for all three functional gene classes. LGD targets in lower IQ affected males are significantly enriched for the FMRP-associated and chromatin-modifier gene classes (Supplementary Table 6). However, for LGD targets in higher IQ males we see no statistically significant enrichment for any of the gene categories.

Target overlaps in children and mutation-type groups

We partitioned children into four primary groups: unaffected siblings, affected females, affected males with higher IQ, and affected males with lower IQ. We analysed these and various combinations for three types of DN mutations: LGDs, missense and synonymous (Supplementary Table 6). Targets of synonymous mutations in all children and targets of LGD and missense mutations in unaffected siblings have no significant overlap with targets from any other group. We see no significant overlap between targets in higher IQ males with targets from other groups. In strong contrast, the 67 LGD targets from affected females overlap significantly with the 166 LGD targets from lower IQ affected males (10 observed, 1.3 expected, $P = 7 \times 10^{-7}$). We therefore refer to the group of lower IQ males and affected females as a 'joint' class. In this class, the 874 missense and 223 LGD targets also overlap significantly (39 observed, 22.1 expected, $P = 0.0008$). Thus, not only do missense and

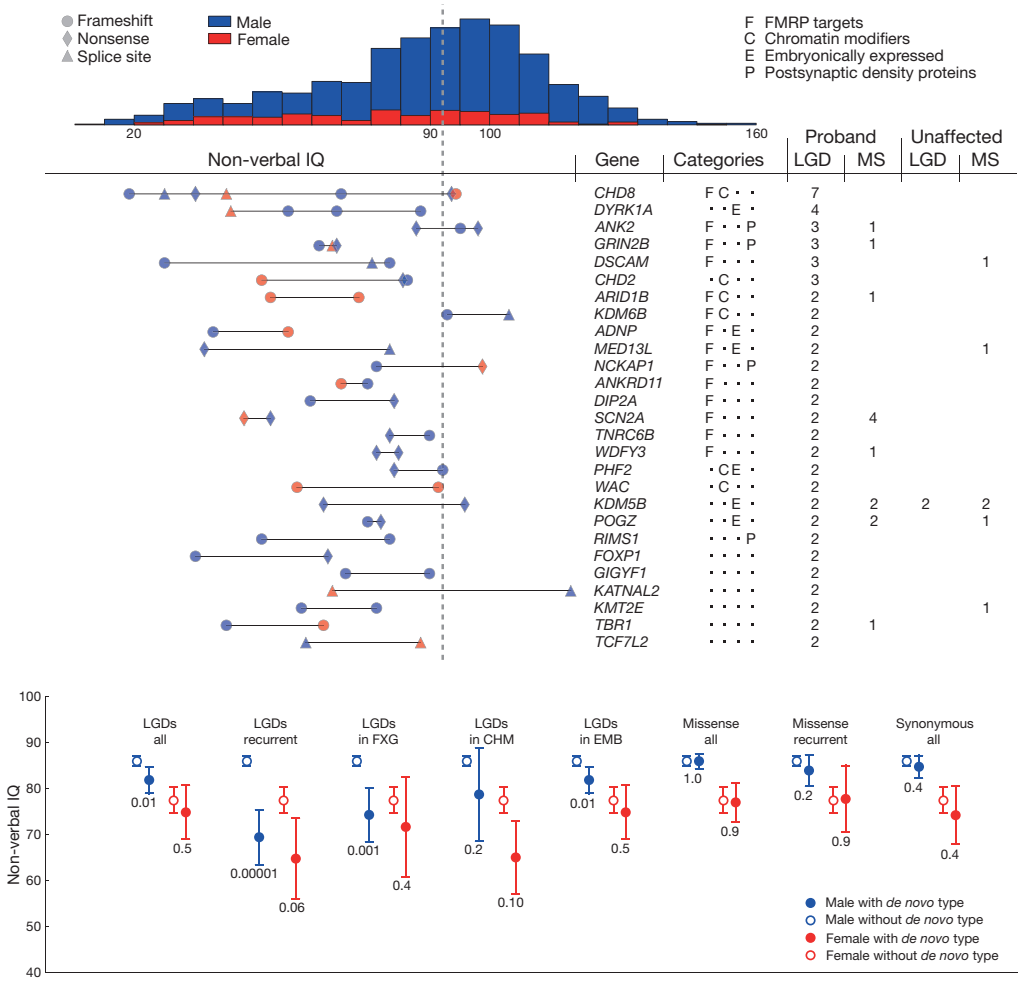

Figure 2 | Recurrently hit genes and non-verbal IQ. Affected females account for 13.5% of the SSC with a mean IQ of 78, whereas affected males have a mean IQ of 86 (top, $P = 10^{-7}$ by Student's *t*-test). Vertical dashed line indicates an IQ of 90. Middle (left) shows IQ for affected children with LGD mutations in genes hit recurrently (right). Recurrently mutated genes are clustered into four categories as shown. The last four columns give overall numbers of DN LGD and missense (MS) mutations. Bottom, eight classes of DN mutations are considered: all LGDs, recurrent LGDs, LGDs in FMRP targets (FXG), LGDs in chromatin modifiers (CHM), LGDs in embryonically expressed genes (EMB), all missense mutations, recurrent missense mutations and synonymous mutations. Probands are divided by the presence of DN mutations and gender. Means, 95% confidence intervals and *P* values (Student's *t*-test) are shown.

LGD mutation target genes with shared functionality, the same genes are sometimes targeted.

Number of vulnerable genes

Our analysis of functional clustering and overlaps within target classes suggests that the mutations ascertained in probands target restricted sets of vulnerable genes. We next sought evidence for excess recurrence of targets. We first examined synonymous mutations and mutations in unaffected children. Among the 647 synonymous events in probands, there are 25 gene targets found in more than one child, close to the null expectation of 19.9 ($P = 0.13$). Recurrent LGD ($n = 3$ out of 179 events) or missense targets (70 out of 1,143 events) in unaffected siblings are

Table 1 | Enrichment of DN mutations in six gene classes

		rDN LGD (ASD)			DN LGD (ASD)			DN miss (ASD)			DN LGD (sib)			DN miss (sib)		
	No. of genes	Overlap (27)			Overlap (353)			Overlap (1,513)			Overlap (176)			Overlap (1,066)		
Gene class		Obs	Exp	*P*	Obs	Exp	*P*	Obs	Exp	*P*	Obs	Exp	*P*	Obs	Exp	*P*
FMRP	842	14	2.6	4×10^{-8}	55	34.1	4×10^{-4}	171	144.8	0.03	14	17.0	0.52	117	102.9	0.15
Chromatin	428	6	0.9	2×10^{-4}	26	11.8	3×10^{-4}	57	50.0	0.31	5	5.9	1.00	37	35.6	0.80
Embryonic	1,912	6	3.4	0.15	65	45.0	2×10^{-3}	220	191.4	0.03	20	22.5	0.65	142	136.0	0.58
PSD	1,445	4	2.5	0.31	34	32.5	0.78	159	138.1	0.07	22	16.2	0.15	113	98.1	0.12
Essential	1,750	7	3.2	0.04	50	42.4	0.22	201	180.3	0.10	20	21.2	0.91	127	128.1	0.96
Mendelian	256	0	0.6	1.00	3	8.0	0.07	31	34.0	0.66	5	4.0	0.61	20	24.1	0.47
DN LGD (Scz)	93	2	0.3	0.03	9	3.7	0.01	16	15.7	0.90	2	1.8	0.71	8	11.2	0.45
DN LGD (ID)	30	3	0.1	1×10^{-4}	8	1.2	3×10^{-5}	10	4.9	0.04	0	0.6	1.00	5	3.5	0.41

We tested eight classes (Methods) for enrichment against five lists of targets of DN mutations. These include genes with (1) recurrent DN LGD mutations in probands (rDN LGD (ASD)); (2) DN LGD mutations in probands (DN LGD (ASD)); (3) DN missense mutations in probands (DN miss (ASD)); (4) DN LGDs in siblings (DN LGD (sib)); and (5) DN missense mutations in siblings (DN miss (sib)). Observed (obs) and expected (exp) numbers are shown with *P* values obtained from two-sided binomial tests. Expected numbers and *P* values are based on a length model in which DN mutations occur randomly in all genes, proportional to length.

also close to null expectations ($P = 0.2$ and 0.04, respectively). In affected males with higher IQ there are no excess recurrent targets among 137 LGDs mutations (2 observed, 1.0 expected, $P = 0.3$) or among 728 missense mutations (26 observed, 24.7 expected, $P = 0.4$). By contrast, among probands the number of recurrent LGD ($n = 27$ out of 391 events) and missense targets (145 out of 1,675 events) are not compatible with the null expectation of 7.6 ($P < 0.0001$) and 115.0 ($P = 0.001$), respectively. Given these findings, as well as the lack of overlap between targets of higher and lower IQ males, we focused on the joint class of female probands and affected males of lower IQ. For the joint class, there were 22 recurrent LGD targets among 254 events with 3.3 expected ($P < 0.0001$). For the 944 missense events, 60 recurrent targets are observed with 40.2 expected ($P = 0.0005$).

We next used recurrence analysis and the length model to estimate the number of vulnerable genes (Fig. 3) and the probability that a recurrent mutation of a given type is contributory (Methods). The most likely number of genes vulnerable to DN mutations in the joint class is estimated to be 387 for LGD targets with a 95% confidence interval of 149–915, and 404 for DN missense targets (confidence interval 71–3,050). From the length model and our estimate that 43% of LGD mutations are contributory, we have 90% confidence that a given LGD mutation contributes to autism in a gene recurrently hit by an LGD mutation (Methods). By the same methods, we compute 35% confidence in contribution from missense mutations in recurrent targets. Using existing models for prioritizing targets[7], we list all targets of recurrent DN coding mutation according to their rank (Supplementary Table 9).

Discussion

The SSC was assembled with the explicit hypothesis that finding targets of DN mutation would be a path to gene discovery. We now have 353 candidate LGD gene targets, 27 genes recurrently hit by LGD events, and 145 recurrent missense targets, each with about 40%, 90% and 35% chance of being contributory, respectively.

We use the ascertainment differential as an estimate of contribution. The sum of the ascertainment differentials for missense, nonsense, consensus splice site disruption and frameshift DN mutations is 0.21 per affected child. Adding 0.06, the ascertainment differential from large DN copy number variants[2,3], brings the total to 0.27 (Fig. 4). Excluding higher IQ males, the value is 0.33. In affected females it is 0.45. This is a conservative estimate for the role of DN mutation in the SSC families because we have not yet ascertained intermediate-size DN copy number variants (CNVs), copy-neutral rearrangements, regulatory mutations or mutations of non-coding genes.

Although the SSC is a simplex collection, it is probably only marginally depleted for high-risk families because small brood size prevents the birth of several affected children, especially if the unaffected sibling is female. We estimate[10] and confirm[9] by gender bias in unaffected siblings (1,400 females and 1,264 males, $P = 0.0089$) that ~40% of the SSC families are high-risk. In a simple genetic model, DN mutation has no role in high-risk families but is obligatory for low-risk families[10], so DN mutation would contribute to ~60% of the SSC. The sum of the ascertainment differential for all observable DN types in all the probands is about 30%, about half of that. If the number of unobserved and consequential DN mutations is similar to the number of observed and consequential DN exome mutations, the actual contribution is not far from that predicted by this simple model.

Targets and cognitive defects

We examined the incidence and targets of DN LGD mutations for children with lower and higher IQs. Affected children with higher IQs have a greater incidence of LGD mutations than unaffected siblings, but a lower incidence than affected females or males with lower IQ. Moreover, there are few recurrently hit genes among the DN LGD targets of affected males with higher IQ, and little overlap with the DN LGD targets of affected males with lower IQ or females. LGD targets in higher IQ males are not enriched for the FMRP-associated genes. These

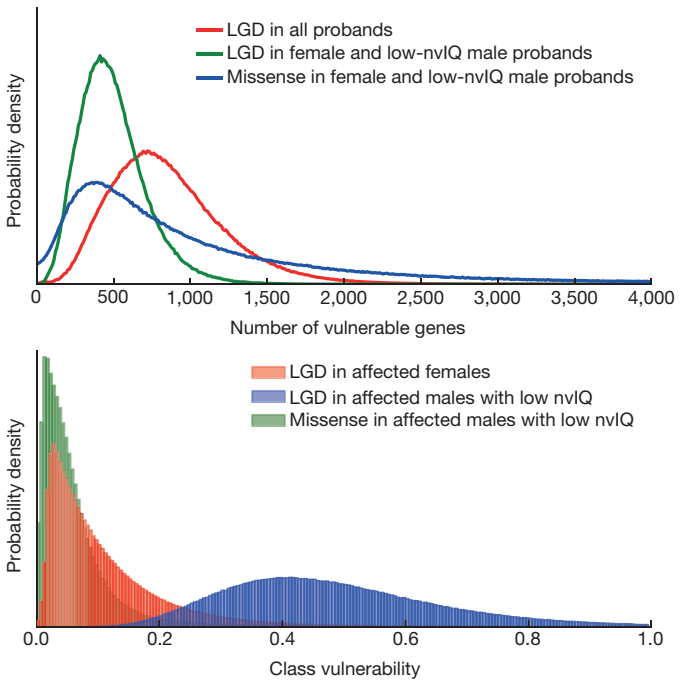

Figure 3 | Number of vulnerable genes and class vulnerability. We assume the property of being vulnerable is independent of gene length, but the probability of being hit by mutation is proportional to gene length. We use the observed rates of mutation of a given type in specified populations and number of recurrent mutations to estimate the number of genes vulnerable to those mutations (top). The degrees of vulnerability in those classes are the distributions shown in the bottom panel (Methods). nvIQ, non-verbal IQ.

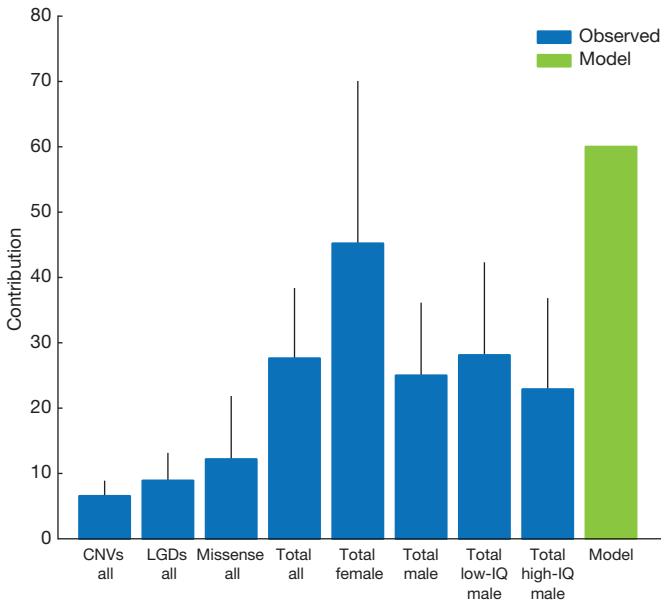

Figure 4 | Estimated contributions of CNVs, LGDs and missense DN mutations to simplex ASD. Ascertainment differentials for three types of DN mutation (CNVs, LGDs and missense) are interpreted as a measure of 'contribution,' the percentage of probands in whom the mutation contributed to diagnosis. We combine the three mutation types in 'total' on the assumption of additivity. We present this measure for 'all' probands and selected subpopulations as indicated. We also show the expected contribution of all DN mutation in a simplex collection computed from a simple genetic model[9] ('model'). Error bars represent 95% confidence intervals.

observations suggest a different distribution of genetic mechanisms underlying ASD in higher IQ males.

We can examine overlap between LGD targets for autism, with published targets for intellectual disability and schizophrenia[25–29]. We applied our length model for mutation incidence and found significant overlap of intellectual disability and schizophrenia targets with ASD targets (Table 1), but only in the joint class of affected males with lower IQ and females (Supplementary Table 6). The overlap can have many explanations: diagnostic conflation; pleiotropy for the same mutation; different consequences for different mutations in the same gene; and varying genetic or environmental background. The DN targets of affected males with higher IQ do not overlap these sets, again suggesting distinct mechanisms.

Properties of target classes

This study is sufficiently large and uniform to enable inferences about targets, distinguished by mutation types, properties of affected children and target functions. We observe a significant contribution from missense mutations, with an overall magnitude comparable to that from LGD mutations. Both LGD and missense mutation targets are enriched in the same functional gene sets, especially among lower IQ males (Supplementary Table 6). Excluding higher IQ males, we estimate the most likely number of genes vulnerable to LGDs is about 400, with a similar number of genes vulnerable to missense. The two sets overlap substantially.

Targets in autism are enriched in certain functional categories, providing deeper support for previously published observations[6–8]. FMRP-associated genes and chromatin modifiers are prominent targets in all groups except higher IQ males. The former are thought to function in neuroplasticity. Embryonically expressed genes are significantly enriched as LGD or missense targets, but only in females. Enrichment in these genes may reflect that these contributory mutations cause alterations before a female protective effect takes place.

Recurrent LGD targets encode receptors, ion channels and synaptic proteins likely to function directly in neuro-circuitry (for example, *SCN2A*, *GRIN2B* and *RIMS1*), but also proteins functioning in cytoskeletal remodelling (for example, *ANK2* and *MED13L*) and transcriptional regulation. Chromodomain helicase gene family members carry many recurrent LGDs. The most frequently hit gene is *CHD8* (ref. 30), followed by *CHD2* (three LGDs) and four other members (one LGD each) of that family. CHD8 is a transcriptional regulator thought to be important for suppression of the Wnt–β-catenin signalling pathway through histone H1 recruitment[31]. Another intriguing target is the protein kinase *DYRK1A*, hit four times and located in the Down's syndrome critical region[7].

Gene vulnerability and molecular mechanisms

We cannot determine the penetrance of specific mutations observed here, as we do not see them often enough in an unselected population. Nevertheless, we introduce the term 'gene vulnerability' as the probability that a given type of mutation in a given gene contributes to a given condition. Genes with non-zero vulnerability define the vulnerable class. We can extend this concept to 'class vulnerability', defined as the mean gene vulnerability over a class of genes. Mathematically, class vulnerability, V, is computed by solving the following equation for V: $F \times A = P \times H \times V$, in which F is the prevalence of the condition, A is the ascertainment differential for DN mutations of a given type in the gene class, P is the expected proportion of the population with DN mutations of that given type, and H is the probability that such mutations hit the gene class.

We can compute a distribution of class vulnerability for all vulnerable genes targeted by a given mutational type (Methods) because F, A and P have empirically sampled distributions and H has a distribution inferred from the total length of the gene class. The distribution of class vulnerability for DN LGDs in males with lower IQ has a mode around 0.4 (Fig. 3). In other words, ~40% of DN LGDs in vulnerable genes in a male contribute to diagnoses of lower IQ ASD. Similarly, ~10% of missense mutations in vulnerable genes contribute to diagnoses of lower IQ autism (Fig. 3). The mode for LGD vulnerability in females is fourfold lower than for lower IQ males, mainly because the prevalence is fourfold lower. Reduced penetrance in females is not well understood, but may be consequent to sexually dimorphic development. Support for this is seen in the relative enrichment of embryonically expressed genes as targets in females.

Partial gene vulnerability can be explained in several ways: some LGD mutations result in autism, some have little effect, and some produce other diagnoses or even lethality. Regardless, many LGD mutations will strongly predispose to ASD. We expect this to be reflected in decreased functional variation in the human gene pool, as we have previously shown for FMRP-associated genes[8].

Given our analysis of gene vulnerability and the lack of evidence for compound heterozygosity, damage to a single allele will often have severe consequences for development. What underlies the vulnerability to haploinsufficiency is unclear. Half the normal gene dosage can result in half the level of gene products, and there are many examples in which physiology requires proper dosage[32–37]. Also, having two copies of a gene will reduce variability of expression[38]. With only one functional allele, there could be increased variation in levels of expression, including dangerously low levels at crucial moments in lineage development, altering the composition of tissues. Monoallelic expression also needs to be considered[39]. Finally, some truncation events might lead to dominant negative alleles.

Present and future implications

From the clinical perspective, early diagnosis and family counselling are complicated if there are hundreds of genetic targets, especially if few are known with certainty. Sequencing of more cohorts is thus clearly warranted. From the therapeutic perspective, the good news is that in almost all cases DN mutations occur in probands in whom a normal allele is also present. It is theoretically possible that enhancing activity of the remaining alleles might alleviate symptoms. So in our view, the long-term prognosis for treating ASD is positive. Moreover, ASD targets overlap with targets for intellectual disability and schizophrenia, so mechanism-based treatments might work for different diagnostic categories. In the intermediate term, functional clustering suggests that treatments might be tailored to a smaller number of convergent pathways.

Online Content Methods, along with any additional Extended Data display items and Source Data, are available in the online version of the paper; references unique to these sections appear only in the online paper.

Received 4 July; accepted 3 October 2014.
Published online 29 October 2014.

1. Jeste, S. S. & Geschwind, D. H. Disentangling the heterogeneity of autism spectrum disorder through genetic findings. *Nature Rev. Neurol.* **10,** 74–81 (2014).
2. Sanders, S. J. *et al.* Multiple recurrent *de novo* CNVs, including duplications of the 7q11.23 Williams syndrome region, are strongly associated with autism. *Neuron* **70,** 863–885 (2011).
3. Levy, D. *et al.* Rare *de novo* and transmitted copy-number variation in autistic spectrum disorders. *Neuron* **70,** 886–897 (2011).
4. Marshall, C. R. *et al.* Structural variation of chromosomes in autism spectrum disorder. *Am. J. Hum. Genet.* **82,** 477–488 (2008).
5. Sebat, J. *et al.* Strong association of *de novo* copy number mutations with autism. *Science* **316,** 445–449 (2007).
6. Sanders, S. J. *et al. De novo* mutations revealed by whole-exome sequencing are strongly associated with autism. *Nature* **485,** 237–241 (2012).
7. O'Roak, B. J. *et al.* Sporadic autism exomes reveal a highly interconnected protein network of *de novo* mutations. *Nature* **485,** 246–250 (2012).
8. Iossifov, I. *et al. De novo* gene disruptions in children on the autistic spectrum. *Neuron* **74,** 285–299 (2012).
9. Ronemus, M., Iossifov, I., Levy, D. & Wigler, M. The role of *de novo* mutations in the genetics of autism spectrum disorders. *Nature Rev. Genet.* **15,** 133–141 (2014).
10. Zhao, X. *et al.* A unified genetic theory for sporadic and inherited autism. *Proc. Natl Acad. Sci. USA* **104,** 12831–12836 (2007).
11. Fischbach, G. D. & Lord, C. The Simons Simplex Collection: a resource for identification of autism genetic risk factors. *Neuron* **68,** 192–195 (2010).
12. Campbell, C. D. *et al.* Estimating the human mutation rate using autozygosity in a founder population. *Nature Genet.* **44,** 1277–1281 (2012).
13. Michaelson, J. J. *et al.* Whole-genome sequencing in autism identifies hot spots for *de novo* germline mutation. *Cell* **151,** 1431–1442 (2012).

14. Schrider, D. R., Hourmozdi, J. N. & Hahn, M. W. Pervasive multinucleotide mutational events in eukaryotes. *Curr. Biol.* **21,** 1051–1054 (2011).
15. Kong, A. *et al.* Rate of *de novo* mutations and the importance of father's age to disease risk. *Nature* **488,** 471–475 (2012).
16. Neale, B. M. *et al.* Patterns and rates of exonic *de novo* mutations in autism spectrum disorders. *Nature* **485,** 242–245 (2012).
17. Darnell, J. C. *et al.* FMRP stalls ribosomal translocation on mRNAs linked to synaptic function and autism. *Cell* **146,** 247–261 (2011).
18. Kang, H. J. *et al.* Spatio-temporal transcriptome of the human brain. *Nature* **478,** 483–489 (2011).
19. Voineagu, I. *et al.* Transcriptomic analysis of autistic brain reveals convergent molecular pathology. *Nature* **474,** 380–384 (2011).
20. Bayés, A. *et al.* Characterization of the proteome, diseases and evolution of the human postsynaptic density. *Nature Neurosci.* **14,** 19–21 (2011).
21. Blake, J. A., Bult, C. J., Kadin, J. A., Richardson, J. E. & Eppig, J. T. The Mouse Genome Database (MGD): premier model organism resource for mammalian genomics and genetics. *Nucleic Acids Res.* **39,** D842–D848 (2011).
22. Feldman, I., Rzhetsky, A. & Vitkup, D. Network properties of genes harboring inherited disease mutations. *Proc. Natl Acad. Sci. USA* **105,** 4323–4328 (2008).
23. Willsey, A. J. *et al.* Coexpression networks implicate human midfetal deep cortical projection neurons in the pathogenesis of autism. *Cell* **155,** 997–1007 (2013).
24. Newschaffer, C. J. *et al.* The epidemiology of autism spectrum disorders. *Annu. Rev. Public Health* **28,** 235–258 (2007).
25. de Ligt, J. *et al.* Diagnostic exome sequencing in persons with severe intellectual disability. *N. Engl. J. Med.* **367,** 1921–1929 (2012).
26. Fromer, M. *et al. De novo* mutations in schizophrenia implicate synaptic networks. *Nature* **506,** 179–184 (2014).
27. Lee, S. H. *et al.* Genetic relationship between five psychiatric disorders estimated from genome-wide SNPs. *Nature Genet.* **45,** 984–994 (2013).
28. McCarthy, S. E. *et al. De novo* mutations in schizophrenia implicate chromatin remodeling and support a genetic overlap with autism and intellectual disability. *Mol. Psychiatry* **19,** 652–658 (2014).
29. Rauch, A. *et al.* Range of genetic mutations associated with severe non-syndromic sporadic intellectual disability: an exome sequencing study. *Lancet* **380,** 1674–1682 (2012).
30. O'Roak, B. J. *et al.* Multiplex targeted sequencing identifies recurrently mutated genes in autism spectrum disorders. *Science* **338,** 1619–1622 (2012).
31. Nishiyama, M., Skoultchi, A. I. & Nakayama, K. I. Histone H1 recruitment by CHD8 is essential for suppression of the Wnt-β-catenin signaling pathway. *Mol. Cell. Biol.* **32,** 501–512 (2012).
32. Birchler, J. A. & Veitia, R. A. Gene balance hypothesis: connecting issues of dosage sensitivity across biological disciplines. *Proc. Natl Acad. Sci. USA* **109,** 14746–14753 (2012).
33. Cooper, D. N., Krawczak, M., Polychronakos, C., Tyler-Smith, C. & Kehrer-Sawatzki, H. Where genotype is not predictive of phenotype: towards an understanding of the molecular basis of reduced penetrance in human inherited disease. *Hum. Genet.* **132,** 1077–1130 (2013).
34. Darnell, J. C. Defects in translational regulation contributing to human cognitive and behavioral disease. *Curr. Opin. Genet. Dev.* **21,** 465–473 (2011).
35. Veitia, R. A., Bottani, S. & Birchler, J. A. Gene dosage effects: nonlinearities, genetic interactions, and dosage compensation. *Trends Genet.* **29,** 385–393 (2013).
36. Weischenfeldt, J., Symmons, O., Spitz, F. & Korbel, J. O. Phenotypic impact of genomic structural variation: insights from and for human disease. *Nature Rev. Genet.* **14,** 125–138 (2013).
37. Zhang, F., Gu, W., Hurles, M. E. & Lupski, J. R. Copy number variation in human health, disease, and evolution. *Annu. Rev. Genomics Hum. Genet.* **10,** 451–481 (2009).
38. Eckersley-Maslin, M. A. & Spector, D. L. Random monoallelic expression: regulating gene expression one allele at a time. *Trends Genet.* **30,** 237–244 (2014).
39. Jeffries, A. R. *et al.* Random or stochastic monoallelic expressed genes are enriched for neurodevelopmental disorder candidate genes. *PLoS ONE* **8,** e85093 (2013).

Supplementary Information is available in the online version of the paper.

Acknowledgements Simons Foundation Autism Research Initiative grants to E.E.E. (SF191889), M.W.S. (M144095 R11154) and M.W. (SF235988) supported this work. Additional support was provided by the Howard Hughes Medical Institute (International Student Research Fellowship to S.J.S.) and the Canadian Institutes of Health Research (Doctoral Foreign Study Award to A.J.W.). E.E.E. is an Investigator of the Howard Hughes Medical Institute. We thank all the families at the participating SSC sites, as well as the principal investigators (A. L. Beaudet, R. Bernier, J. Constantino, E. H. Cook Jr, E. Fombonne, D. Geschwind, D. E. Grice, A. Klin, D. H. Ledbetter, C. Lord, C. L. Martin, D. M. Martin, R. Maxim, J. Miles, O. Ousley, B. Peterson, J. Piggot, C. Saulnier, M. W. State, W. Stone, J. S. Sutcliffe, C. A. Walsh and E. Wijsman) and the coordinators and staff at the SSC sites for the recruitment and comprehensive assessment of simplex families; the SFARI staff for facilitating access to the SSC; and the Rutgers University Cell and DNA Repository (RUCDR) for accessing biomaterials. We would also like to thank the CSHL Woodbury Sequencing Center, the Genome Institute at the Washington University School of Medicine, and Yale Center for Genomic Analysis (in particular J. Overton) for generating sequencing data; E. Antoniou and E. Ghiban for their assistance in data production at CSHL; and T. Brooks-Boone, N. Wright-Davis and M. Wojciechowski for their help in administering the project at Yale. The NHLBI GO Exome Sequencing Project and its ongoing studies produced and provided exome variant calls for comparison: the Lung GO Sequencing Project (HL-102923), the WHI Sequencing Project (HL-102924), the Broad GO Sequencing Project (HL-102925), the Seattle GO Sequencing Project (HL-102926) and the Heart GO Sequencing Project (HL-103010).

Author Contributions CSHL: I.I., M.R. and M.W. designed the study; I.I., D.L., B.Y., Y.L., E.G., E.D., P.A., A.L., J.K., G.N., S.Y., M.C.S., K.Y. and M.W. analysed the data; M.R., I.H., J.R., B.M., L.R., J.T. and W.R.M. generated the exome data at Cold Spring Harbor Laboratory; I.I., Z.W., S.M. and J.T. confirmed the variants; I.I., M.R. and M.W. wrote the paper. UCSF/Yale: S.J.S. and M.W.S. designed the study; S.J.S., S.D., L.W. and A.J.W. analysed the data; S.J.S., J.D., L.E.G., J.D.M., C.A.S., M.F.W. and Z.W. confirmed the variants; S.M.M. and M.T.M. generated the exome data at Yale Medical Center. UW: B.J.O., J.S. and E.E.E. designed the study; B.J.O. and N.K. analysed the data; B.J.O., H.A.S., K.T.W. and L.V. confirmed the variants; E.E.E. and J.S. revised the manuscript; K.E.P, J.D.S., B.P. and D.A.N. generated the exome data at the University of Washington.

Author Information Sequence data used in these work are available from the National Database for Autism Research (http://ndar.nih.gov/), under study DOI:10.15154/1149697. Reprints and permissions information is available at www.nature.com/reprints. The authors declare competing financial interests: details are available in the online version of the paper. Readers are welcome to comment on the online version of the paper. Correspondence and requests for materials should be addressed to J.S. (shendure@uw.edu), E.E.E. (eee@gs.washington.edu), M.W.S. (matthew.state@ucsf.edu), or M.W (wigler@cshl.edu).

METHODS

Sample collection. Most families (2,517) came from current or former members of the SSC. The SSC was assembled at 13 clinical centres, accompanied by detailed and standardized phenotypic analysis as reported previously[11]. Several IQ measures (verbal, non-verbal and full spectrum) were recorded; in this work, we stratified probands by non-verbal IQ, which we refer to as simply 'IQ' throughout the text. Families with single probands and unaffected siblings were preferentially recruited, whereas families with two probands were specifically excluded[11]. Families from two associated collections were also sequenced: the Simons Ancillary Collection (SAC, $n = 123$), and the Simons Twin Collection (STC, $n = 13$). The SAC includes families that failed inclusion criteria for the SSC, typically because a parent, sibling or second- or third-degree relative of the affected participant has been diagnosed with ASD, or for cases in which the proband's ASD diagnosis was questionable. The STC consists of families of monozygotic twins in which at least one co-twin is affected by ASD. The institutional review boards of Cold Spring Harbor Laboratory, Yale Medical Center and University of Washington, Seattle approved this study. Written informed consent from all subjects was obtained by SFARI. Blood samples were drawn from parents and children (affected and unaffected) and sent to the Rutgers University Cell and DNA Repository (RUCDR) for DNA preparation. DNAs from 2,517 families (of ~2,800 total in the SSC) were used in this study. Results from 774 of the SSC families included here were published in earlier work[6–8]. The samples were split across the three centres: Cold Spring Harbor Laboratory (CSHL), the Department of Genetics at the Yale School of Medicine (YALE), and Department of Genome Sciences at the University of Washington (UW). The split was not uniform with respect to number of families or the proportions of female probands and probands with lower IQ (Extended Data Fig. 2 and Supplementary Table 1). Several families were sequenced at multiple centres, with 24 families sequenced in all three centres (Extended Data Fig. 1 and Supplementary Table 1).

Exome capture, sequencing and validation. The three centres differed in the precise exome capture platform, read length and validation protocols.

CSHL. The protocols described previously[8] were applied to the families newly sequenced at CSHL. In brief, SeqCap EZ Human Exome Library v2.0 (Roche NimbleGen) reagents were used with a custom barcoding protocol that enabled simultaneous exome enrichment of ≤4 genomes and the sequencing of ≤8 individuals per Illumina HiSeq 2000 lane. All exome sequencing was performed using paired-end 100-base pair (bp) reads. All strong and weak LGD candidate variants as well as additional variants from families sequenced at CSHL were subjected to experimental validation. Gene-specific primers were designed for PCR amplification of candidate single nucleotide variables (SNVs) and indels, and amplicons were pooled and sequenced on an Illumina MiSeq. Approximately 100 variants were validated per lane with paired-end 150-bp reads. Where possible, the parental origin was determined by phasing of linked transmitted SNVs.

UW. Samples were captured and sequenced by one of three methods. In the pilot set (19 quads), samples were captured using SeqCap EZ Human Exome Library v1.0 (Roche NimbleGen) reagents (UW-M1)[7,40]. The remaining samples were captured using SeqCap EZ Human Exome Library v2.0 (Roche NimbleGen) reagents[7]. Newly sequenced samples were either processed as described previously[7] (UW-M2) or with a modified (UW-M3) protocol (Supplementary Table 10). For UW-M2, single-plex captures and single-plex sequencing runs (non-pooled) were performed as described previously[7]. For UW-M3, single-plex capture was performed as in UW-M2; however, in the post-capture PCR, an 8-bp index barcode was added. Post-PCR libraries were quantified and pooled in sets of ~96. These pools were then sequenced on the Illumina MiSeq platform to evaluate library complexity and sample distribution. Pools were rebalanced on the basis of performance, then sequenced across multiple HiSeq 2000 lanes using paired-end 50-bp reads. Additional lanes were added until samples reached target coverage (20×: ~80%; 8×: ~90%). If additional coverage was required for some samples, subpools were also generated. For samples processed with UW-M1 and UW-M2, predicted *de novo* calls were validated using standard PCR and Sanger sequencing[7]. For UW-M3 processed samples, custom Molecular Inversion Probe (MIP) capture probes were designed with targeting arms flanking regions of interest. Probes were designed without or with degenerate tags, and pools of ~50–100 probes were generated[30,41]. As described earlier[41], sets of families (~96 samples) were captured using these pools with 50–100 ng of genomic DNA as template. Capture products were then pooled and sequenced on an Illumina MiSeq. Candidate sites failing MIP QC or capture, or showing evidence of significant shifts in allele balance, were validated using the standard PCR/Sanger method. If sites repeatedly failed the assay, they were discarded. Novel sites called by the CSHL pipeline were validated using the same methods as UW-M3.

YALE. Whole blood-derived genomic DNA was enriched for exonic sequences using SeqCap EZ Human Exome Library v2.0 (Roche NimbleGen) reagents. All family members were barcoded and each pool of four samples was sequenced using 75-bp paired-end reads on single lanes of the Illumina HiSeq 2000 instrument. Where possible, all four family members were sequenced on the same lane to minimize batch effects. All strong and weak LGD candidate variants from the CSHL pipeline, along with an additional set of LGD candidates from the Yale pipeline, were subjected to experimental validation as follows: variant-specific primers were designed for PCR amplification of candidate SNVs and indels from all family members, and amplicons were sent for Sanger sequencing.

Sequence analysis pipelines. Sequence data were interpreted as family genotypes using pipeline tools at each respective data centre. Almost all of the data were reanalysed with the CSHL pipeline. We show the coverage (Extended Data Fig. 6) and yields (Extended Data Fig. 7) for *de novo* calls from each centre. The 24 families sequenced at all three centres demonstrated good agreement between pipelines and platforms (Supplementary Tables 11 and 12).

The analysis pipelines generated candidate *de novo* events, defined as variants present in the child and absent in both parents. We filtered out variants seen frequently in the parents of the collection (allele frequency >0.3%), reasoning that most of these would be false positives owing to uneven coverage in a parent. Candidates generated by local pipelines or by the common CSHL pipeline were validated at the respective centres with re-sequencing and 2,504 were verified. In our final call set, we include all verified calls from each centre, and omit any call that was rejected. In addition, because almost all (1,640 of 1,644) strong point mutations generated by the common CSHL pipeline were verified when successfully tested (Supplementary Table 11), such strong candidates are included in our call set even if the validation test failed or if the candidate event was not tested. All frameshift mutations were validated, and we exclude all that were rejected. All *de novo* calls used in the subsequent analysis, along with their validation status, are listed in Supplementary Table 2. Pipelines for analysis and validation were blind with respect to affected and unaffected status.

CSHL (uniform) pipeline. Sequence data from the three centres were analysed with the computational pipeline described previously[8]. In brief, the Illumina analysis pipeline (CASAVA 1.8) was used for base calls, and custom software was used to de-multiplex reads and trim barcodes from CSHL derived data. Data from Yale and UW were de-multiplexed at the respective centres before analysis through the CSHL pipeline. BWA[42] was used to align sequence reads to the hg19 reference genome, and both Picard (http://broadinstitute.github.io/picard/) and GATK[43] were used for marking PCR duplicates, family-based sequence realignment and quality score recalibration. As described previously, a multinomial model-based family genotyper was used to generate candidate SNV and indel 'Mendel violators,' each annotated with: (1) a confidence score (denovoScr) that reflects the posterior probability of Mendel violation at the locus; (2) a goodness-of-fit score (chi2Score) showing the degree to which the assumptions of the multinomial model are applicable to the observed data; (3) counts of reads per allele and per family member; and (4) allele frequency and noise rates for the candidate position based on the whole collection. Candidates SNVs with denovoScr ≥60 and chi2Score >0.0001 were labelled 'strong' provided that the position was not polymorphic or noisy in the population, and that the parents were homozygous for the reference allele.

For SNVs, a cut-off denovoScr value of 60 was dictated by the desire to keep false positives to a minimum, and was chosen after computing the proportion of *de novo* candidates that appear at polymorphic loci (a surrogate for false positives) as a function of the score (see the Supplement of ref. 8). The low false positive rate (<5%) was also confirmed through experimental validation (Supplementary Table 11). In addition, we observe that only 1% of DN mutations are shared between two siblings (Supplementary Table 2), putting a 3% cap on false positives owing to failure to observe parents correctly. At stringent thresholds the false negative rate is generally high, but through simulations we determined that, even with stringent thresholds, regions with deep coverage (40× or higher joint coverage) had low false negative rates (<5%).

Indels were treated differently than SNVs. The multinomial model assumes a small allele bias, appropriate when calling SNVs, but not for *de novo* indels—particularly for long events (>10 bp). To address this, cut-offs for 'strong' indels were lowered (denovoScr >30 and chi2Score $>10^{-9}$). To reduce noise, we added requirements for 'clean' read counts: parents were not allowed to have any reads containing the candidate indel, and were required to have at least 15 reads supporting the reference allele. At least one of the children had to have ≥6 reads with the candidate variant, and those reads had to comprise ≥5% of reads. Experimental validation demonstrated that the false positive rate in the strong indels is <10%, and simulations for indels without extreme allele bias (most of those <10 bp) reveal that the false negative rate in well-covered regions (40×) is <5%.

All 'strong' SNVs and indels are reported here unless rejected by validation. To address the high false negative rates, we defined a class of 'weak' SNV and indels drawn from thresholds lower than strong candidates. All weak LGD candidates were subjected to validation, and only those successfully validated are reported. In addition, during method development (for example, through manual inspection or see ref. 44), we validated a large number of candidates that did not meet even

the weak definition. Candidate variants found as valid under these circumstances are reported here and labelled as 'not called'. This label is also used when the CSHL uniform pipeline missed a call from the UW and YALE data that was successfully validated.

UW pipeline. All samples using UW-M1 and UW-M2 protocols were processed as described earlier[7]. For UW-M3, updated versions of BWA (0.5.9-r16), Picard-tools (1.48) and GATK (1.0-6125) were used. The GATK Unified Genotyper was used in single sample mode with filter flags (AB > 0.75, low quality, QD < 5.0, QUAL ≤ 50.0) and in parallel with the SAMtools pipeline as described previously[40] (see the GATK Unified Genotyper for definitions of these scores). Only positions with ≥8-fold coverage were considered. Child genotype calls were compared to the parental genotypes to identify possible *de novo* events. Predicted DN SNVs were analysed against a set of 946 exomes to remove recurrent artefacts and likely undercalled sites. Indels were also called with the GATK Unified Genotyper and SAMtools[45], and included only those with ≥25% of reads showing a variant at a minimum depth of 8×. These were then filtered against a larger set of 1,779 exomes (as with SNVs). Those sites passing (that is, not present) in the exome screen and also not present in multiple UW-M3 processed families were manually evaluated by inspecting alignments in the Integrative Genomics Viewer (http://www.broadinstitute.org/igv/home). Sites with obvious misalignments (for example, non-gapped indels or soft-clipped only reads) were removed. Moreover, if reads supporting the predicted DN mutation were present in ≥5% of 20 (or more) reads in one of the parents, the site was excluded. For sites with lower coverage, a variant was excluded if present in ≥10% (for example, 1 in 10, or 2 in 20) of parent reads or (for quads) if at least one variant read was present in one parent and the other child.

Yale pipeline. The Yale data were analysed as described previously[6]. In brief, CASAVA 1.8 was used for demultiplexing and base calling, reads were aligned to hg19 with BWA[42], and SAMtools[45] was used for marking PCR duplicates and genotyping. In-house scripts were used for family-based assessment of *de novo* mutations and annotation against genes and the exome variant server (http://varianttools.sourceforge.net/Annotation/EVS).

Null models for target overlaps and recurrence. We introduce the term mutation-child-type to refer to a set of events of a certain mutational type (for example, missense or LGD) in children of a certain type (for example, male affected individuals with higher IQ or unaffected siblings). We observe target enrichment in gene classes, and document overlaps and recurrence between and within mutation-child-types. To measure significance, we use a null model in which the probability that a gene is hit by mutation is proportional to its length, a model supported by observation (Extended Data Fig. 5). We examine the distributions of lengths of gene targets of *de novo* synonymous, missense and LGD mutation in affected children and siblings. These distributions are compared to simulations of genes picked at random or in proportion to their length. The data fit well with the model that mutation frequency is linearly dependent on gene length. The group with the largest deviation from this rule is the set of DN targets in affected children, both for missense ($P = 0.001$) and for LGDs ($P = 0.001$, Supplementary Table 13). These P values are defined as the probability that the median length of the target class can arise under the null model, and are computed by simulations of equal number of genes weighted by length. Although the deviation is statistically significant, it is of such a minor amount that we ignore it for the null model.

Measuring overlaps. We test for overlaps between targets of a given mutation-child-type and other sets of genes (for example, overlap of DN LGD targets in affected girls with FMRP-associated genes) as well as overlaps between targets of two different mutation-child-types (for example, overlap between the targets of DN missense in all probands and the targets of DN LGDs in all probands). In both cases, observed overlaps are compared to those expected under the length-based null model discussed above.

Let T be the targets of mutation of a given type in a child of a given type, S a predefined gene set, and O the intersection of T and S. We ask for any gene G that carries a single mutation, what the probability $p(S)$ is that the mutation (and hence G) falls in S. We estimate $p(S)$ by collapsing all recurrent hits to one, and applying the length-based null model to S. Thus $p(S)$ is the ratio of (1), the sum of exome-captured lengths of the genes of S, divided by (2), the sum of the exome-captured lengths of all genes. Supplementary Table 7 shows the length of the captured portion of all genes in the exome we analyse. Using '||' to designate the number of members in a set, we then perform a two-sided binomial test of $|O|$ outcomes in $|T|$ opportunities given the probability of success $p(S)$.

When we test overlaps between targets of two different mutation-child-types, we take one of the targets as T and compare the other targets as S. However, before constructing T and S, we cleanup targets shared by T and S that result from mutations shared between siblings in the same family, or from multiple mutations of different types affecting a single gene in one child. We then apply the method of the paragraph above. Finally, we reverse the procedure for creating of S and T, and report both results (Supplementary Table 6).

Test for excessive recurrence. If we have R recurrent genes in K events in a mutation-child-type class, we test for excess recurrence by comparing R to the number of recurrent genes expected under the gene length-based null model. We build the expectation by performing 10,000 simulations. In each simulation, we sample K genes with replacement where the probability of sampling a gene is proportional to its length. We then count the number of recurrences.

Estimation of the number of vulnerable genes. To estimate the number of vulnerable genes for a given mutation-child-type, we start with the observed number of events (K), the observed number of recurrent events (R), the estimated posterior distributions for the rates of mutations of the given type in the ascertained (Mdist) and for the unaffected (Pdist) population. We then explore possible number of vulnerable genes (T) from 1 to 4,000. For each T, we estimate (through a simulation described in the next paragraph) the likelihood $L(T) = P(R|T,\text{Mdist},\text{Pdist},K)$. Assuming all numbers of vulnerable genes from 1 to 4,000 are equally likely, we compute a posterior distribution of the number of genes $p(T)$ proportional to $L(T)$ and determine the maximum value and 95% confidence intervals.

To estimate the likelihood, $L(T) = P(R|T,\text{Mdist},\text{Pdist},K)$, we perform 10,000 simulations for every T. In each simulation:

(1) We randomly select T distinct vulnerable genes from all genes, without respect to length. Unlike mutation, which strikes a gene according to its length, we assume that the chance a gene can cause autism if mutated is independent of its length.

(2) We select the number N of contributory events by sampling from a binomial distribution Binom(K,A/M), where P a randomly selected rate from Pdist, M is a randomly selected from Mdist, $A = M - P$ is a sampled ascertainment differential, and A/M is an estimate of the proportion of contributory events.

(3) We simulate N contributory mutation events by selecting N events with replacement from the T vulnerable genes proportional to their length.

(4) To simulate random events, we select $K - N$ genes from all well-covered genes with replacement proportional to their length.

(5) We record the number of recurrent events in the K selected events from above.

We set $L(T) = P(R|T,\text{Mdist},\text{Pdist},K)$ to be the proportion of simulations in which the number of recurrent events is exactly R. $P(T)$ is obtained by normalizing $L(T)$. For every simulation in which the number of recurrent events is exactly R, we also record the proportion of contributory events among the recurrent events, and the vulnerability point estimate as discussed in the next section.

Vulnerability. We use the equation described in the text: $F \times A = P \times H \times V$, in which F is the prevalence of the given condition in the population, A is the ascertainment differential for DN mutations of a given type in persons ascertained for that condition, P is the expected proportion of the population with such DN mutations, H is the probability that such a mutation hits the target, and V is the mean class vulnerability. These variables are in fact random variables with empirically derived distributions.

We first demonstrate the method for computing the class vulnerability point estimate for genes vulnerable to LGD mutations for the ASD males of lower IQ, assuming that the variables are fixed. One in 75 males is diagnosed with autism, and we estimate (from empirically derived gender biases) that three-quarters of these males are of lower IQ, yielding a prevalence $F = 1/100$. From our study, 0.23 of these have an LGD. Because the expected proportion of people with a DN LGD mutation is $P = 0.11$, only $A = 0.12$ of this subpopulation have an LGD in a vulnerable gene that contributes to ascertainment. Thus $F \times A = 1.2 \times 10^{-3}$ is the proportion of males that have lower IQ and autism resulting at least partially from a DN LGD. This proportion is also given by $P \times H \times V$, in which H is the probability that the LGD hits within the genes vulnerable to LGD mutations, and V is the mean class vulnerability for these genes. P, as already stated, is 0.11. We have computed the number of genes vulnerable to LGD mutations, N, for the affected males with lower IQ to be about 400 genes (Supplementary Table 6). Assuming membership in the target class is independent of gene length, and about 20,000 genes, we calculate $H = 400/20{,}000 = 0.02$, and solve V to be 0.55.

We assume the following prevalence: $F = 1/75$ for ASD in males, $F = 1/100$ for ASD with lower IQ in males, $F = 1/300$ for ASD with higher IQ in males, and $F = 1/300$ for ASD in girls. A and P are empirically derived gamma distributions from the sampled Poisson rates of DN LGD mutations in affected and unaffected siblings. By keeping the observed number of LGD events and the observed proportion of LGD events constant, we sample from the distribution of target number N and the distributions on A and P as described in the previous section. We set H to be the ratio of the total length of uniformly sampled vulnerable genes to the total length of the analysed captured exome, and compute a vulnerability point estimate as described just above. These sampled values are displayed in Fig. 3, bottom. The mode for V is 0.4 for males of lower IQ.

Parental age and phasing of DN mutations. We used two different strategies for modelling the relationship between rates of DN substitutions and the ages of the parents.

The first strategy does not depend on knowledge of the parent of origin for DN substitutions, which we do not know for the vast majority of DN substitutions. Because the ages of the mother and the father are strongly correlated, we can effectively use this strategy only to explore the relationship between the father's age and the rates of DN substitutions. Over probands and siblings in the 40× -joint family target, we model the number of mutations per child as sampled from a Poisson distribution with rate $R_c = T_c \times (A \times F_c + B)$, in which R_c is the rate of DN substitutions per child, F_c is the age of the father at the birth of the child, T_c is the ratio of the length of the 40×-target in that child to the total exome length, and A and B are whole population parameters, estimated by maximizing the likelihood over all children.

The second strategy is applicable only to DN mutations for which we have successfully 'phased' the parent of origin by proximity to a linked polymorphism. For each parental gender, we separately perform a two-sided one-sample t-test to compare the parental ages of each phased DN mutation to the mean of parental ages in our population.

DN substitutions increase ~0.4 per paternal decade (Extended Data Fig. 4), consistent with previous studies[15] and the increase in autism as a function of paternal age[46,47]. Where we could determine parental phase, DN substitutions arose more frequently in the paternal (287) than in the maternal (80) background. Among phased DN events, the mean age at birth was 34.6 for the father and 32.0 years for the mother, whereas the respective mean ages were 33.2 and 31.1 years for fathers and mothers in the whole population ($P = 0.0001$ and 0.047, respectively, that these differences arise by chance).

Gene class definition. For determining overlap with *de novo* mutations, functional gene classes were defined as follows. 'FMRP' are genes encoding transcripts that bind to FMRP[17]. 'Chromatin' indicates chromatin modifiers as defined by Gene Ontology (GO; http://www.geneontology.org/). 'PSD' is a set of genes encoding proteins that have been identified in postsynaptic densities[20]. 'Mendelian' represent positionally identified human disease genes[22], and 'essential' genes are human orthologues of mouse genes associated with lethality in the Mouse Genome Database[21]. 'dn LGD (Scz)' are *de novo* LGDs in schizophrenia[26,48,49] and 'dn LGD (ID)' are *de novo* LGDs in intellectual disability[25,29].

'Embryonic' genes are those expressed in post-mortem human embryonic brains[19], derived from downloaded expression data[18] (http://www.brainspan.org/static/download.html). This data set provides normalized expression levels for ~17,000 genes across brain regions from 36 individuals, 18 of which were from embryos. Each brain was further subdivided into 14 anatomical regions for a total of 508 regions. We computed correlation values for the 17,000 genes, and generated a graph by connecting genes that had correlations >0.85, then identified connected components and averaged the expression of genes within these components as a function of the annotated age of the brain and by region. Each region is sorted first by age, then by type (Extended Data Fig. 8). The averaged normalized expression of the 1,912 genes in the first component decreases after birth, and hence we call this set embryonic.

Supplementary Table 7 shows the genes in the eight functional classes that are within the captured exome regions and were used in all analyses.

40. O'Roak, B. J. *et al.* Exome sequencing in sporadic autism spectrum disorders identifies severe *de novo* mutations. *Nature Genet.* **43,** 585–589 (2011).
41. Boyle, E. A., O'Roak, B. J., Martin, B. K., Kumar, A. & Shendure, J. MIPgen: optimized modeling and design of molecular inversion probes for targeted resequencing. *Bioinformatics* **30,** 2670–2672 (2014).
42. Li, H. & Durbin, R. Fast and accurate short read alignment with Burrows–Wheeler transform. *Bioinformatics* **25,** 1754–1760 (2009).
43. McKenna, A. *et al.* The Genome Analysis Toolkit: a MapReduce framework for analyzing next-generation DNA sequencing data. *Genome Res.* **20,** 1297–1303 (2010).
44. Narzisi, G. *et al.* Accurate *de novo* and transmitted indel detection in exome-capture data using microassembly. *Nature Methods* **11,** 1033–1036 (2014).
45. Li, H. *et al.* The Sequence Alignment/Map format and SAMtools. *Bioinformatics* **25,** 2078–2079 (2009).
46. Reichenberg, A. *et al.* Advancing paternal age and autism. *Arch. Gen. Psychiatry* **63,** 1026–1032 (2006).
47. Croen, L. A., Najjar, D. V., Fireman, B. & Grether, J. K. Maternal and paternal age and risk of autism spectrum disorders. *Arch. Pediatr. Adolesc. Med.* **161,** 334–340 (2007).
48. Gulsuner, S. *et al.* Spatial and temporal mapping of de novo mutations in schizophrenia to a fetal prefrontal cortical network. *Cell* **154,** 518–529 (2013).
49. Xu, B. *et al.* Exome sequencing supports a de novo mutational paradigm for schizophrenia. *Nature Genet.* **43,** 864–868 (2011).

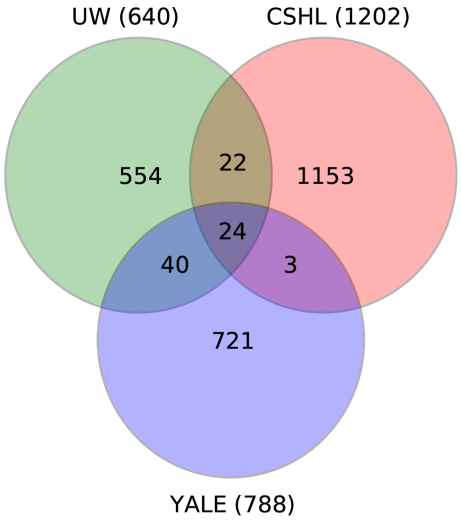

Extended Data Figure 1 | Number of families sequenced by centre. The numbers of families sequenced at the three centres are plotted as a Venn diagram. Families sequenced at more than one centre are indicated by the overlapping regions between circles. CSHL, Cold Spring Harbor Laboratory; UW, University of Washington, Seattle; YALE, Yale Medical Center.

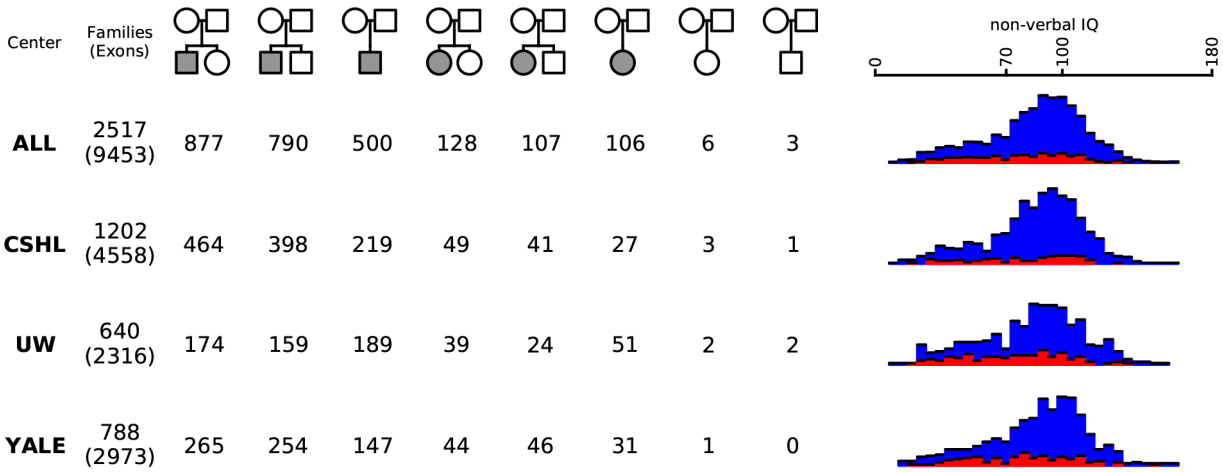

Extended Data Figure 2 | SSC sequencing by pedigree type and non-verbal IQ. A summary of all SSC families sequenced is indicated across the 'all' row. Numbers of SSC families with complete exome sequencing data are displayed by centre in the following rows (see Extended Data Fig. 1 legend for centre designations). The top number in entries under the 'families' column indicates the total number of families sequenced, and the number in parentheses below indicates the total number of individuals. Family pedigree structures are shown across the top row with gender indicated by shape (square for male, circle for female) and affected status indicated by colour (white for unaffected, grey for affected). Distributions of non-verbal IQ within each cohort are shown for male probands (blue) and female probands (red).

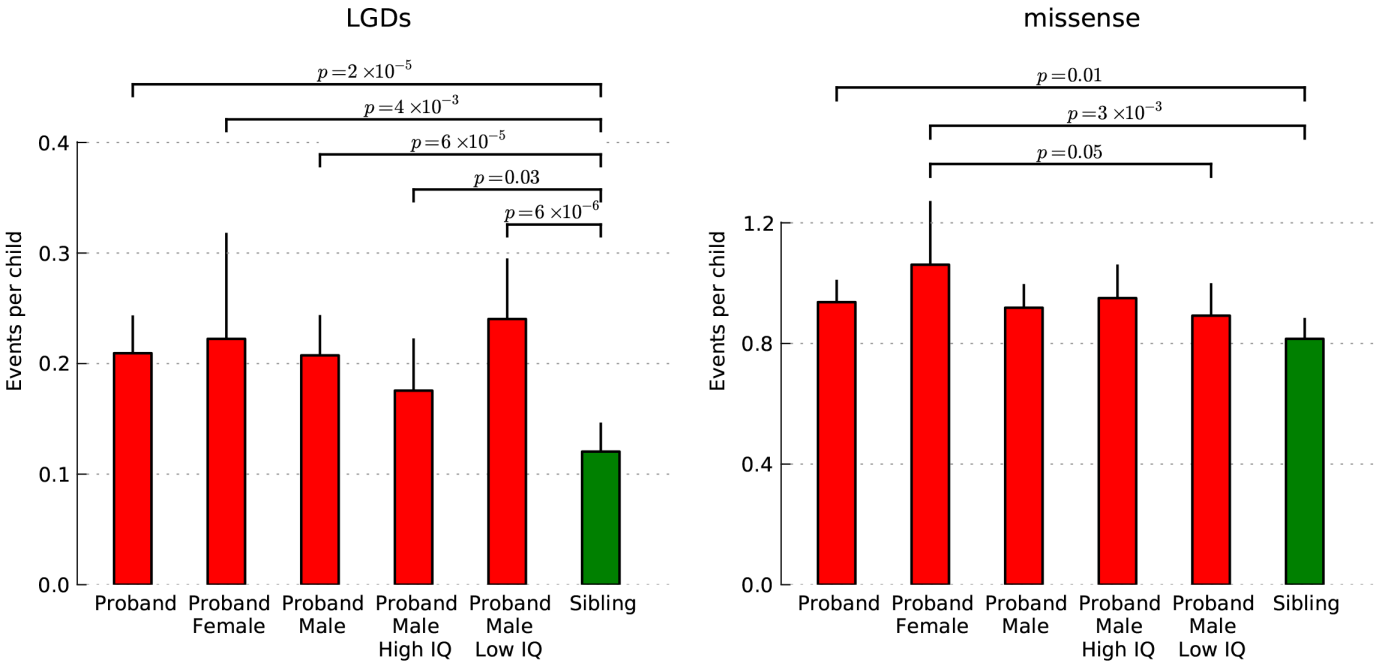

Extended Data Figure 3 | Rates of *de novo* LGD and missense mutations in the SSC by child status. On the left we show the LGD rate per child in six types of children, labelled on the *x* axis, defined by their affected status, gender, and non-verbal IQ. We test for equal rates for every pair of child types and we show the ones with $P > 0.05$ with thin lines on the top of the figure. Although not significant, the rates in affected females and in affected males of lower non-verbal IQ are larger than the rate in males of higher non-verbal IQ. On the right, we show the missense rates per child for the same six groups of children.

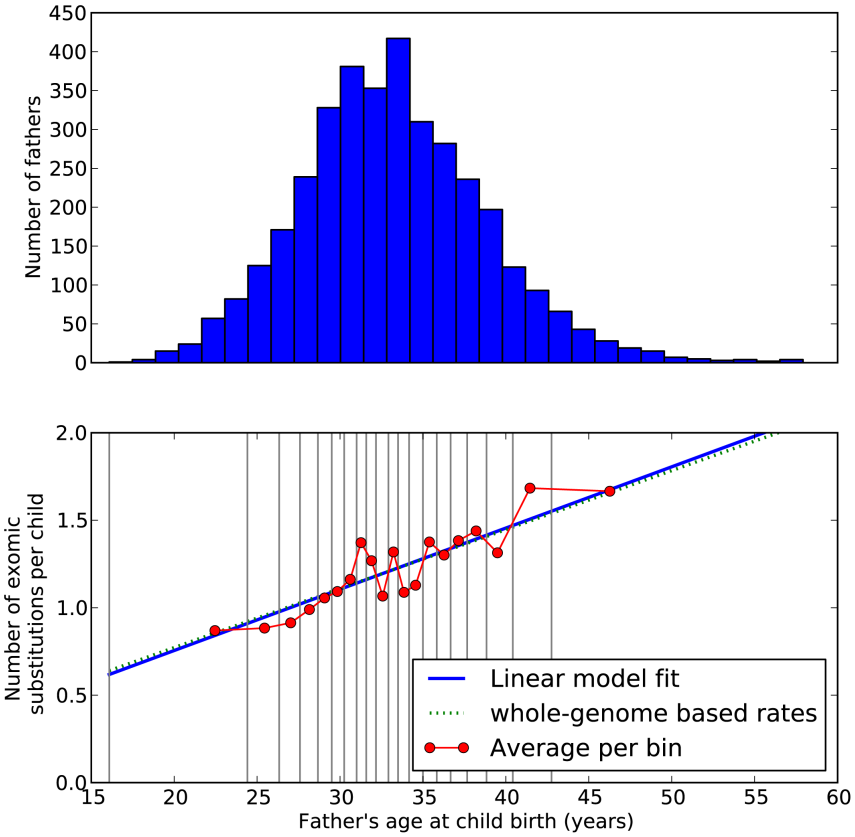

Extended Data Figure 4 | Paternal age and DN mutation rate at child birth. Distribution of paternal age at birth of children (top) and rates of DN mutation in offspring as a function of paternal age are shown (bottom). Children were ordered by paternal age at birth and split into 20 groups of similar size, as shown in the bottom panel. The red curve shows the mean observed rates of *de novo* exomic substitutions in each of the 20 groups, with the *x* coordinate equal to the mean each of the fathers' ages within each group. The blue line shows a linear fit to the observed rates. The dotted green line represents DN mutation rates from whole genome sequencing data[15] scaled to rates per exome based on representation in the SeqCap EZ Human Exome Library v2.0 (Roche NimbleGen).

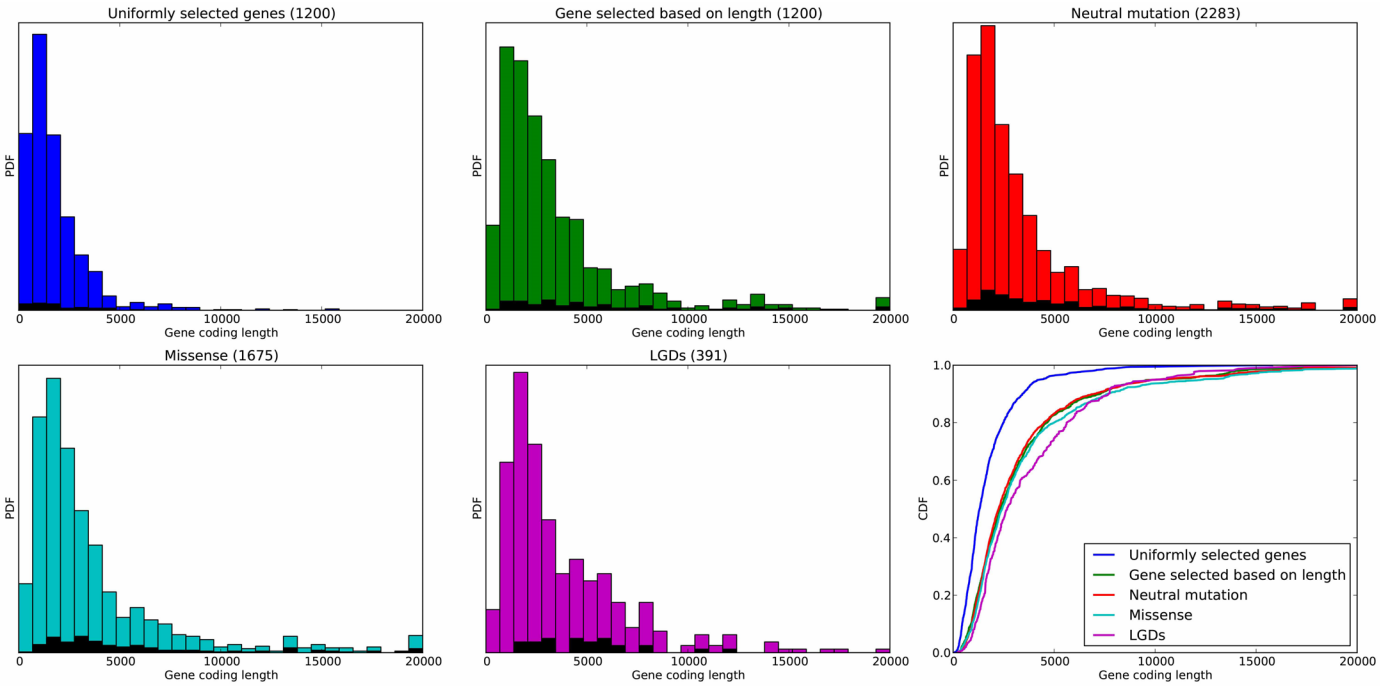

Extended Data Figure 5 | Coding region size distribution for query sets of genes. Probability density function (PDF) and cumulative distribution functions (CDF) (right bottom) of the distributions of the coding region length in base pairs of five sets of genes: a set of 1,200 genes picked uniformly from the set of exome-targeted genes (blue); a separate set of 1,200 genes picked with probabilities proportional to length of the coding region (green); the set of gene targets of neutral mutations, including synonymous mutations in probands and siblings, and missense mutation in siblings (red); genes with *de novo* missense mutations in probands (cyan); and genes with *de novo* LGDs in probands (magenta). Black within the histograms shows the distribution of lengths of the recurrently hit genes from each class. Coding region length distribution under a uniform model does not fit the lengths of the genes with observed mutations, and genes with LGD mutations are longer than predicted by a simple length-based model (bottom right).

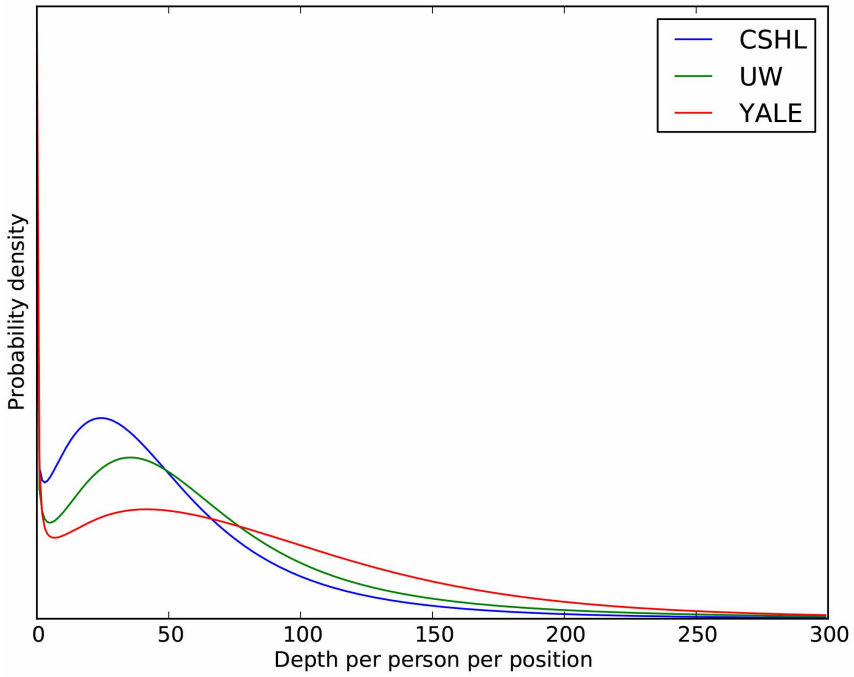

Extended Data Figure 6 | Distributions of sequencing depth. Distributions of sequencing depth (number of sequence reads covering a given genomic position) per person per position for the three sequencing centres are plotted. Centre designations are as in Extended Data Fig. 1.

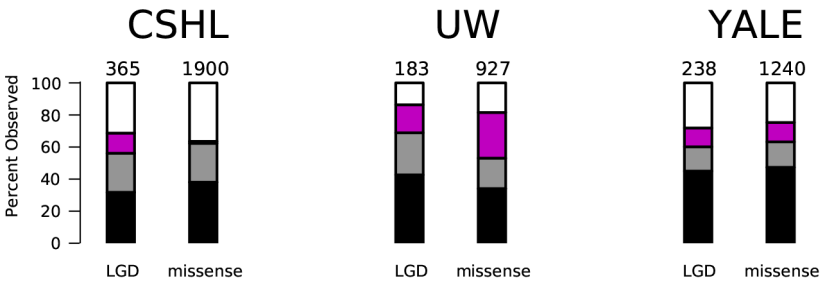

Extended Data Figure 7 | Yield of DN LGD and missense mutations. We plot the yield of DN LGD and missense mutations per sequencing centre (designations as in Extended Data Fig. 1). In each case we show the number of mutations we expect to see based on the estimated rates per child, indicated by the numbers above the bars. We also show what percentage of the expected number we have observed. Black refers to strong calls in the 40× target, grey refers to strong calls outside of 40× target, and magenta refers to weak (but valid) calls. The white region represents the difference between the expected and observed numbers of variants.

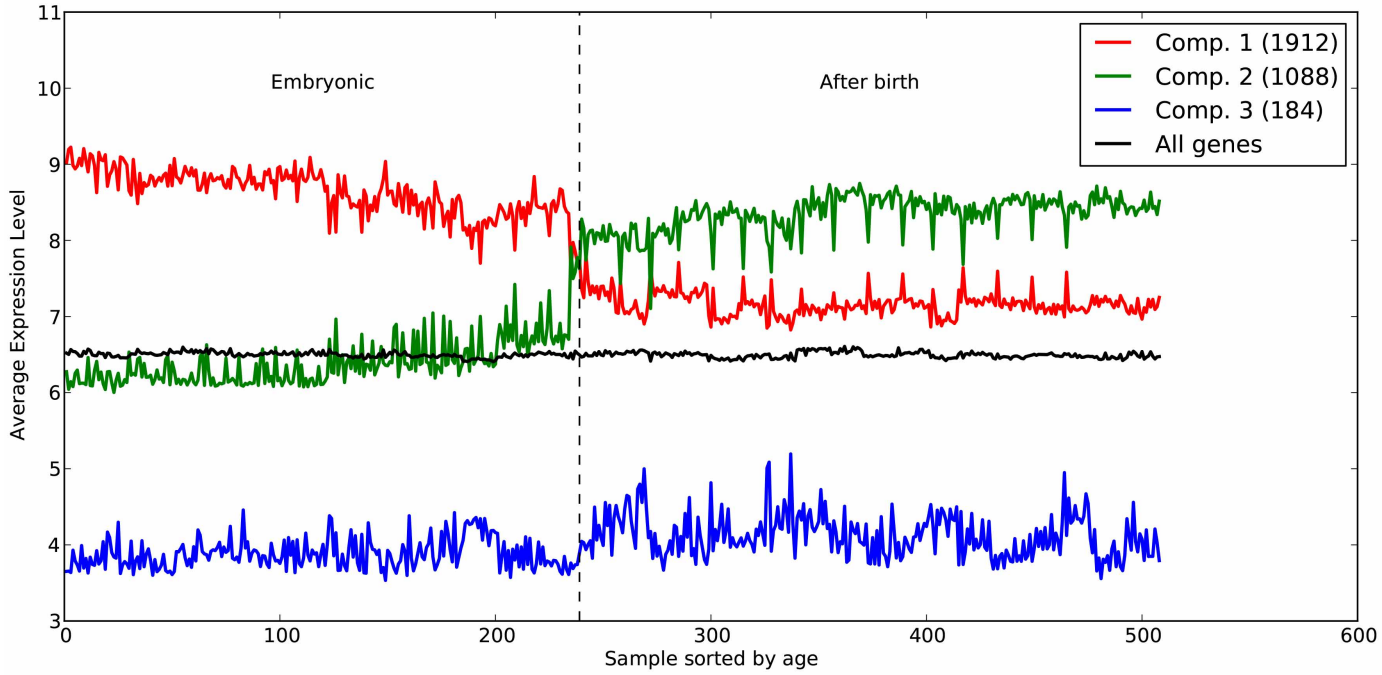

Extended Data Figure 8 | Categorization of embryonically expressed genes. We downloaded expression data[18] from http://www.brainspan.org/static/download.html. The data set provides normalized expression levels for ~17,000 genes across brain regions from 36 individuals, 18 of which were from embryos. Each brain was further subdivided into 14 anatomical regions for a total of 508 regions. We computed correlation values for the 17,000 genes, and generated a graph by connecting genes that had correlations >0.85. We then identified connected components and averaged the expression of genes within these components as a function of the annotated age of the brain and by region. Each region is sorted first by age, then by type. The averaged normalized expression of the 1,912 genes in the first component decreases after birth, and hence we call this set embryonic. See Supplementary Table 7 for the list of embryonic genes.